JOURNAL OF SPACECRAFT AND ROCKETS
Vol. 41, No. 5, September–October 2004

# Navier–Stokes Computation of Pitch–Damping Coefficients Using Steady Coning Motions

Soo Hyung Park* and Jang Hyuk Kwon†
*Korea Advanced Institute of Science and Technology, Daejeon 305-701, Republic of Korea*

**A prediction method for pitch–damping force and moment coefficients is presented in the unified framework of the unsteady Navier–Stokes equations with the $k$–$\omega$ turbulence equations. This approach does not require modification of the governing equations other than the addition of noninertial force terms. The present method is applied to compute the pitch–damping coefficients using the lunar coning and the zero-spin coning motions. Grid refinement and parametric studies are performed. The computed pitch–damping coefficients and Magnus moment coefficients are in good agreement with both the parabolized Navier–Stokes data and the experimental data. The direct unsteady predictions are performed and compared with the steady coning motions. The results show that the present steady and unsteady approaches can be successfully applied to the prediction of the pitch–damping coefficients.**

## Nomenclature

| | | |
|---|---|---|
| $A_{\text{ref}}$ | = | reference area $\pi D^2/4$, m$^2$ |
| $C_m$ | = | pitching moment coefficient |
| $C_{m_q} + C_{m_{\dot\alpha}}$ | = | pitch–damping moment coefficient (sum), $(2U_\infty/D)(\partial C_m/\partial\dot\alpha)$ |
| $D$ | = | reference length (base diameter), m |
| $e$ | = | total energy, nondimensionalized by $p_\infty/\rho_\infty$ |
| $\boldsymbol{F}$ | = | inviscid flux vectors |
| $\boldsymbol{F}_v$ | = | viscous flux vectors |
| $J$ | = | Jacobian |
| $k$ | = | reduced frequency for harmonic pitching motion, $q_0 D/\alpha_0 U_\infty$; turbulent kinetic energy in the turbulence equations |
| $M$ | = | Mach number |
| $Pr$ | = | Prandtl number |
| $Pr_t$ | = | turbulent Prandtl number |
| $p$ | = | pressure nondimensionalized by $p_\infty$; spin rate, rad/s |
| $q$ | = | pitch rate, rad/s |
| $\boldsymbol{q}$ | = | conservative flow variable vector |
| $\boldsymbol{R}$ | = | flux residual vector |
| $\boldsymbol{R}^U$ | = | unsteady residual vector |
| $\boldsymbol{S}_{k\omega}$ | = | source vector of the $k$–$\omega$ equations |
| $T$ | = | nondimensional period for a cycle |
| $\boldsymbol{T}$ | = | right eigenvector matrix |
| $t$ | = | physical time, s |
| $t^*$ | = | nondimensional physical time, $(t/D)\sqrt{(p_\infty/\rho_\infty)}$ |
| $U$ | = | freestream speed, m/s |
| $\boldsymbol{U}$ | = | contravariant velocities |
| $\boldsymbol{U}_g$ | = | grid or frame velocity vector |
| $u, v, w$ | = | nondimensional velocity components in $x$, $y$, and $z$ directions |
| $x, y, z$ | = | Cartesian coordinates |
| $\alpha$ | = | angle of attack, deg |
| $\alpha_m$ | = | mean angle of attack, deg |
| $\alpha_t$ | = | total angle of attack $\sqrt{(\alpha^2+\beta^2)}$, deg |
| $\alpha_0$ | = | amplitude of angle of attack, deg |
| $\alpha^*$ | = | angle of attack for harmonic motion, deg |
| $\beta$ | = | side-slip angle, deg |
| $\gamma$ | = | the ratio of specific heats |
| $\boldsymbol{\Lambda}$ | = | diagonal matrix of eigenvalues |
| $\mu_l$ | = | laminar viscosity determined by Sutherland's law |
| $\mu_t$ | = | turbulent eddy viscosity, $0.09(\rho k/\omega)$ |
| $\xi, \eta, \zeta$ | = | generalized coordinates |
| $\rho$ | = | density, nondimensionalized by $\rho_\infty$ |
| $\tau$ | = | pseudotime |
| $\boldsymbol{\Omega}$ | = | angular velocity vector of the rolling frame |
| $\omega$ | = | nondimensional frequency, $\sqrt{(\gamma)}M_\infty k$; specific dissipation rate in the turbulence equations |

*Subscript*

| | | |
|---|---|---|
| $\infty$ | = | freestream condition |

*Superscripts*

| | | |
|---|---|---|
| $\cdot$ | = | rate of change with respect to time |
| $\tilde{}$ | = | referenced to body-fitted coordinate frame |
| $n, m$ | = | time-step levels |

Received 21 April 2003; presented as Paper 2003-3671 at the 21st Applied Aerodynamics Conference, Orlando, FL, 23–26 June 2003; revision received 31 July 2003; accepted for publication 1 August 2003. 

*Research Associate, Department of Aerospace Engineering.
†Professor, Department of Aerospace Engineering, 373-1 Guseong-dong, Yuseong-gu. Senior Member AIAA.

## Introduction

MUCH of the static and dynamic performances of projectiles have been obtained through semi-empirical methods and experiments. Computational methods for the prediction of dynamic damping coefficients, such as pitch– or roll–damping coefficients, were proposed comparably later. Because an experiment can be simulated by direct unsteady computation, unsteady methods in the inertial coordinate frame enable us to compute the damping forces and moments directly without any theoretical assumptions and geometrical constraints.[1] However, unsteady methods are time consuming and are not recommended for practical predictions except for prediction of special projectile shapes and conditions.

Since Tobak et al.[2] outlined the aerodynamics of a body in a coning motion, the steady coning motions in noninertial rotating framework have been commonly used to predict pitch–damping coefficients.[3–6] More recently, Weinacht et al.[7] proposed an approach to predicting the individual components of the pitch–damping coefficients sum by using the helical motions (see Ref. 8). Deficiencies of these methods are that they require the Magnus force or moment[9] to be explicitly determined from other sources and that they sometimes require a geometrical constraint such

as axisymmetry.[6] Despite having these deficiencies, the steady methods provide a cost-effective approach to aerodynamics associated with unsteady or time-dependent motions.

Previous steady methods are based on the relationship between the pitch–damping coefficients and the side forces and moments due to coning motions.[2] The methods used noninertial cylindrical formulations, which are appropriate in describing axisymmetric flows. Therefore, the governing equations, with both complex source terms due to coordinate transformation and noninertial force terms, have been written in the cylindrical coordinate frame.[3,6] The noninertial formulation written in the Cartesian coordinate frame has been used in describing rotating flows with constant rotation rates, such as turbomachinery and rotor-blade flows.[10–12] It is argued in this paper that the steady coning motions to predict the damping coefficient can be defined in the framework of the Cartesian coordinate frame. The present approach requires the noninertial force terms only to be added to the unsteady solver,[1] whereas a steady solution method is needed to predict the pitch–damping coefficients.

In this paper, a discussion of the theoretical approach is presented first. The three-dimensional Navier–Stokes equations combined with the $k$–$\omega$ turbulence equations are applied to compute the flowfields.[13] The pitch–damping force and moment coefficients are predicted using the lunar coning and the zero-spin coning (combined spinning and coning) motion. When the steady and direct unsteady methods are used, the pitch–damping forces and moments of axisymmetric Army–Navy spinner rocket (ANSR) geometries[6] are computed and compared. Grid refinement and parametric studies also are performed.

## Theoretical Approach

The pitch–damping coefficients can be obtained by steady or unsteady flow simulations for the specified motions. To describe the unsteady method for predicting the damping coefficients, the specified unsteady motions producing damping moments should be defined. The pitch–damping moment sum can be obtained from the forced harmonic pitching motion about the center of gravity in a rectilinear flight. The planar pitching motion is defined by the angle of attack and pitch rate as a function of time as

$$\alpha(t^*) = \alpha_m + \alpha_0 \sin\left(\sqrt{\gamma} M_\infty k t^*\right) \tag{1}$$

$$q(t^*) = \dot{\alpha}(t^*) = q_0 \cos\left(\sqrt{\gamma} M_\infty k t^*\right) \tag{2}$$

where the pitch rate $q_0$ at the mean angle of attack is $(\alpha_0 U_\infty k)/D$. In a rectilinear motion, the angular rates $q$ and $\dot{\alpha}$ are equal, and the pitch–damping coefficients can be summed and treated as a single coefficient. The moment coefficients for the pitching motion can be expanded with the first-order terms for the rates as follows:

$$C_m(t^*) = C_m|_{\alpha_m} + C_{m_\alpha} \cdot \alpha(t^*) + (D/2U_\infty)[C_{m_q} + C_{m_{\dot{\alpha}}}] \cdot \dot{\alpha}(t^*) \tag{3}$$

If $\alpha_0$ is small and the variation of the pitch–damping moment coefficients sum is small near the angle of $\alpha_m$, the coefficients sum can be determined by integrating Eq. (3):

$$C_{m_q} + C_{m_{\dot{\alpha}}}|_{q=q_0} = \left(\frac{2U_\infty}{D}\right) \frac{\int C_m \, \mathrm{d}\alpha}{\int \dot{\alpha} \, \mathrm{d}\alpha}$$

$$= \frac{2\sqrt{\gamma} M_\infty}{\pi \alpha_0} \int_0^T C_m \cos\left(\sqrt{\gamma} M_\infty k t^*\right) \mathrm{d}t^* \tag{4}$$

Previously, Tobak et al.[2] built up the nonlinear theory of bodies in coning motions and showed that the linear pitch–damping coefficients are related to the side forces and moments due to coning motions. The linear relation between the side moment and the pitch–damping moment coefficient is expressed as moment components in the coning coordinate frame ($\tilde{}$) in Fig. 1. The positive $\tilde{x}$ axis of the nonrolling coordinate frame is orientated toward the base, and the $\tilde{y}$ and $\tilde{z}$ axes are orientated perpendicular to the $\tilde{x}$ axis. Detailed

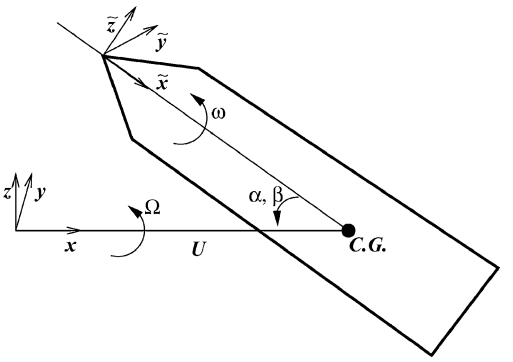


**Fig. 1 Schematic of coning motion and coordinate frames.**

derivation of the relationship may be found in Refs. 3 and 6. The moment formulation in the $\tilde{x}$–$\tilde{z}$ plane can be expanded as follows:

$$\tilde{C}_m + i\tilde{C}_n = C_{m_\alpha}\delta + i\delta\left\{(pD/2U_\infty)C_{n_{p\alpha}} + (\Omega D/2U_\infty)\left[C_{m_q} + C_{m_{\dot{\alpha}}}\right]\right\} \tag{5}$$

The total side moment (imaginary part) consists of contributions from the Magnus moment and pitch–damping moment.

To confirm the aerodynamic theory, Schiff[3] solved the steady Euler equations to compute the supersonic inviscid flow around the body in coning motion. The computation was based on the finding that the flow is steady if a rotating coordinate frame is used. He adopted a "lunar coning" motion to determine the pitch–damping coefficients from the side moments computed. For the steady lunar coning motion, the coning frame and the body rotate at the same angular velocity. Therefore, there is no rotation of the pitch plane with respect to the body, that is, $p = \Omega \cos\alpha_t$. Then, the side moment expression can be written as

$$\tilde{C}_n = \delta(\Omega D/2U_\infty)\left\{\cos\alpha_t C_{n_{p\alpha}} + \left[C_{m_q} + C_{m_{\dot{\alpha}}}\right]\right\} \tag{6}$$

Steady flow modeling techniques can be applied to determine the flowfield due to steady lunar coning motion under the constraint that both the coning rate and the angle of attack are small. The lunar coning motion can also be applied for both the axisymmetric and nonaxisymmetric bodies. This approach was employed in determining the pitch–damping coefficients for supersonic finned projectiles.[5]

The problem with the lunar coning motion[6] is that the side moment is proportional to the sum of the pitch–damping moment sum and the Magnus moment. When it is assumed that the Magnus moment coefficient $C_{n_{p\alpha}}$ can be explicitly determined, this relation will allow the pitch–damping coefficient to be determined. Neglecting the Magnus moment is possible because it is small compared with the pitch–damping moment sum, especially in supersonic flows. This lunar coning approach is thought of as an excellent engineering method for predicting the pitch–damping coefficients of finned projectiles. If the Magnus moment cannot be neglected in the case of a finned projectile, it must be determined from other sources, such as an experiment or a direct unsteady simulation.[9]

To determine the pitch–damping moment sum directly, Weinacht et al.[6] proposed the "combined spinning and coning" motion that allows the side moment to be proportional to the pitch–damping moment only. For the steady combined spinning and coning motion, the body rotates in the coning frame with a rate of rotation that is proportional to the coning rate, $\omega = -\Omega \cos\alpha_t$. Consequently, the spin rate of the body is zero, $p = 0$, and the side moment can be written as

$$\tilde{C}_n = \delta(\Omega D/2U_\infty)\left[C_{m_q} + C_{m_{\dot{\alpha}}}\right] \tag{7}$$

This combined spinning and coning motion is referred to as the zero-spin coning motion in this paper. Because the rotation of the body in the coning frame will produce a time-dependent boundary condition and flowfield, this method is only a steady method for axisymmetric bodies and requires a Navier–Stokes code to implement the boundary condition correctly.

The theoretical relationships between the side and damping moments have been derived from the fact that the flowfield is potentially steady in the nonrolling frame for the coning motion. The side moment can be obtained in both the cylindrical and Cartesian coordinate frames. Because the side moment can be determined uniquely provided that the specified total angle of attack is given, several researchers prefer using the cylindrical coordinate frame. As shown in Ref. 7, however, the governing equations have additional complicated source terms and initial conditions considering axis rotation. If the coning motions can be specified in Cartesian coordinates, the governing equations and solution methods would be simpler and less stiff. The current effort concentrates on using the Cartesian coordinate frame to predict the side moments due to the coning motions.

## Numerical Methods

### Governing Equations

The steady Navier–Stokes equations in the rotating coordinate frame can be described in the framework of the unsteady Navier–Stokes equations with different definitions for the relative velocity.[10,11] In this paper, the three-dimensional compressible full Navier–Stokes equations and Wilcox's $k$–$\omega$ turbulence equations (see Refs. 14 and 15) are considered over a control volume $\mathcal{V}(t)$. The detailed viscous formulation can be found in Refs. 13 and 15:

$$\frac{\mathrm{d}}{\mathrm{d}t}\int_{\mathcal{V}(t)} \boldsymbol{Q}\,\mathrm{d}\mathcal{V} + \int_{\partial\mathcal{V}(t)} (\boldsymbol{F}-\boldsymbol{F}_v)\,\mathrm{d}\mathcal{S} = \int_{\mathcal{V}(t)} \left(\boldsymbol{S}_{k\omega} + \alpha^F \boldsymbol{H}\right)\mathrm{d}\mathcal{V} \quad (8)$$

with

$$\boldsymbol{Q} = [\rho,\ \rho u,\ \rho v,\ \rho w,\ \rho e,\ \rho k,\ \rho\omega]^T \quad (9)$$

$$\boldsymbol{F} = \begin{bmatrix} \rho\boldsymbol{U} \\ \rho u\boldsymbol{U} + n_x p \\ \rho v\boldsymbol{U} + n_y p \\ \rho w\boldsymbol{U} + n_z p \\ (\rho e + p)\boldsymbol{U} + p\boldsymbol{U}_g \\ \rho k\boldsymbol{U} \\ \rho\omega\boldsymbol{U} \end{bmatrix} \quad (10)$$

$$\boldsymbol{H} = [0, \boldsymbol{h}\cdot\hat{\boldsymbol{i}}, \boldsymbol{h}\cdot\hat{\boldsymbol{j}}, \boldsymbol{h}\cdot\hat{\boldsymbol{k}}, \boldsymbol{h}\cdot\boldsymbol{u}, 0, 0]^T \quad (11)$$

$$\boldsymbol{h} = -\rho[\boldsymbol{\Omega}\times\boldsymbol{u}] \quad (12)$$

$\boldsymbol{U}$ means the relative flow velocity at the control surfaces in each direction:

$$\boldsymbol{U} = n_x u + n_y v + n_z w - \boldsymbol{U}_g \quad (13)$$

where $\boldsymbol{U}_g$ is the grid velocity in the inertial coordinate frame or the frame velocity in the noninertial rotating coordinate frame. If a planar pitching motion is enforced in the inertial frame, $\boldsymbol{U}_g$ is defined as the grid velocity of the moving grid. On the other hand, $\boldsymbol{U}_g$ is set to the frame velocity of the coordinate frame rotating at a constant angular velocity when the steady equations with Eq. (11) are solved. Accordingly, to compute the damping coefficients using the steady methods in the noninertial coordinate frame, the parameter $\alpha^F$ is set to one only when the steady governing equations are solved.

This formulation for the governing equations[10–12] is different from the previous formulation in the cylindrical coordinate frame.[3,6] The cylindrical formulation has advantages for axisymmetric flowfields, whereas implementing the noninertial coordinate system in the previously developed unsteady flow solver is much easier with the Cartesian formulation. In addition, the Cartesian formulation does not require the additional source terms caused by the cylindrical coordinate transformation. The remaining question is what the frame velocities are in applying specified noninertial motions.

The damping coefficients can be computed in a similar manner if suitable coning motions are defined in each coordinate system. The total angle of attack $\alpha_t$ and coning rate $\boldsymbol{\Omega}$ should be defined for the coning motion in cylindrical coordinates, whereas either $\alpha$ or $\beta$ should be chosen in the Cartesian coordinates. Therefore, the side moment in Eq. (6) or Eq. (7) is equal to the moment with respect to the $\tilde{y}$ or $\tilde{z}$ axis. In this work, the following set of input data for the coning motion is used unless otherwise stated:

$$\alpha = 2, \qquad \beta = 0, \qquad \boldsymbol{\Omega} = [\Omega_c\cos\alpha,\ 0,\ \Omega_c\sin\alpha]^T \quad (14)$$

and freestream conditions are specified as

$$\rho = 1, \qquad \rho u = \sqrt{\gamma}M_\infty\cos\alpha\cos\beta$$
$$\rho v = \sqrt{\gamma}M_\infty\cos\alpha\sin\beta, \qquad \rho w = \sqrt{\gamma}M_\infty\sin\alpha$$
$$\rho e = 1/(\gamma-1) + \tfrac{1}{2}\gamma M_\infty^2 \quad (15)$$

To fulfill the conservation laws in the Cartesian coordinates, Eqs. (14) and (15) must be defined so that the following Eq. (16) is satisfied at the far field:

$$[\boldsymbol{\Omega}\times\boldsymbol{u}]_{r\to\infty} = 0 \quad (16)$$

Equation (8) can be discretized with the cell-centered finite volume method and integrated cellwise in the computational space domain. To compute the residual over each cell, the HLLE + scheme[16] is used and the third-order monotone upstream scheme for conservation laws interpolation method, MUSCL, with the van Albada limiter is adopted to obtain second-order accuracy (see Ref. 17). The HLLE + scheme has been designed as an improvement in the family of Godunov-type schemes. It is robuster and more accurate than the Roe scheme for supersonic viscous flows. Although the governing equations are no longer in conservation form because of the noninertial force term, the shock-capturing property of the scheme is hardly affected because the Mach numbers applied are not so large as to produce strong stiffness.

### Multigrid Diagonalized Alternating Direction Implicit Method

Dual-time stepping with the diagonalized alternating direction implicit (DADI) method[1,18] is used to advance the solution in time. This allows one not only to use a large time increment but also to maintain temporal accuracy. The dual-time stepping also eliminates factorization and linearization errors by iterating the solutions along a pseudotime.[19] The time derivative for the physical time is approximated by the backward difference discretization to be second order, and so the governing equations become

$$\boldsymbol{R}^U_{ijk} = \frac{3\boldsymbol{q}^{n+1}_{ijk} - 4\boldsymbol{q}^{n}_{ijk} + \boldsymbol{q}^{n-1}_{ijk}}{2J\,\Delta t^*} + \boldsymbol{R}^{n+1}_{ijk} = 0 \quad (17)$$

Here it is convenient to define a new residual $\boldsymbol{R}^U$. Equation (17) can be considered as the equation of the steady-state problem by introducing a derivative with respect to a pseudo-time $\tau$. The pseudo-time problem can be solved by using any time-marching methods which have been proposed to solve steady-state problems, as well as any of the convergence acceleration techniques.[19] In this work, the DADI method[18] is used to find steady-state solutions. An implicit pseudo-time-stepping method[20] can be written as

$$\left[\left(\frac{1}{J\,\Delta\tau} + \frac{3}{2J\,\Delta t^*}\right)\boldsymbol{I} + \frac{\partial\boldsymbol{R}}{\partial\boldsymbol{q}}\right]\Delta\boldsymbol{q} = -\boldsymbol{R}^U_{ijk}(\boldsymbol{q}^m) \quad (18)$$

By the use of the ADI method, Eq. (18) can be factored as follows:

$$\{\boldsymbol{D}+\boldsymbol{A}_\xi\}\boldsymbol{D}^{-1}\{\boldsymbol{D}+\boldsymbol{A}_\eta\}\boldsymbol{D}^{-1}\{\boldsymbol{D}+\boldsymbol{A}_\zeta\}\Delta\boldsymbol{q} = -\boldsymbol{R}^U \quad (19)$$

where

$$\boldsymbol{D} = (1/J\,\Delta\tau + 3/2J\,\Delta t^*)\boldsymbol{I} \quad (20)$$

Here $\boldsymbol{A}_i = (\partial\boldsymbol{R}/\partial\boldsymbol{q})$ in each direction is the Jacobian matrix of a residual, which differs according to the spatial discretization

method.[18] Finally, Eq. (19) can be expressed in a DADI form by using the similarity transformation

$$\left\{\boldsymbol{D} + \nabla^- \Lambda_\xi^+ + \nabla^+ \Lambda_\xi^- - \bar{\delta}_\xi^2 r\left(A_{v_\xi}\right)\right\}\boldsymbol{D}^{-1}$$

$$\left\{\boldsymbol{D} + \nabla^- \Lambda_\eta^+ + \nabla^+ \Lambda_\eta^- - \bar{\delta}_\eta^2 r\left(A_{v_\eta}\right)\right\}\boldsymbol{D}^{-1}$$

$$\left\{\boldsymbol{D} + \nabla^- \Lambda_\zeta^+ + \nabla^+ \Lambda_\zeta^- - \bar{\delta}_\zeta^2 r\left(A_{v_\zeta}\right)\right\} \cdot \Delta \boldsymbol{q} = -\boldsymbol{R}^U \qquad (21)$$

where $\nabla^\pm$ are the backward and forward difference operators and where the $\bar{\delta}_i^2 r(A_{vi})$ operators express the central differencing of viscous fluxes. Note that the contribution of viscous terms is not simultaneously diagonalizable, contrary to the inviscid one. The contributions of viscous terms must be added in the implicit part only by the following approximation of the spectral radius scaling:

$$r(A_v) = 2(\mu_l/Pr_l + \mu_t/Pr_t)(\gamma/\rho) \qquad (22)$$

Furthermore, the source vector $\boldsymbol{S}_{k\omega}$ of the turbulence equations must be implicitly treated because it results in the stiffness problem of time-marching methods.[15]

A loosely coupled algorithm is used for integrating the Navier–Stokes and the $k$–$\omega$ equations separately. It has been widely used to implement many turbulence model equations, although a fully coupled algorithm[15] would be faster than a loosely coupled one. The use of an efficient multigrid algorithm reduces the number of pseudotime iterations as well as the computing time of steady solutions. To implement the multigrid on the DADI method with the dual-time-stepping method, some modifications are applied to the standard saw-tooth cycle algorithm.[19] Note that the strongly nonlinear terms can not preserve the accuracy in the coarse levels because the velocity gradients can significantly alter the magnitude of the source terms. As such, it is important to freeze the nonlinear terms to preserve the turbulence variables in the coarse levels.[15] A more detailed description may be found in Ref. 13.

#### Boundary Conditions

Supersonic inflow is fixed to the freestream values and outflow is extrapolated from the values at the interior cells. The freestream $\omega$ is set to $\mathcal{O}(10U_\infty/D)$ proposed by Menter.[21] The freestream eddy viscosity is set to $0.009\mu_l$ and the turbulent kinetic energy can be calculated from the definition of the eddy viscosity. It is well known that $k$–$\omega$ models have freestream dependence.[21] For the cases considered, freestream dependence is not an important effect and, so, is not considered in this study.

At the solid walls, no-slip conditions for velocities are applied, and the density and energy are extrapolated from the interior cells. It has been found that the difference between the adiabatic and constant wall temperature conditions is negligible for the Mach numbers considered. For the cases with spin, the tangential velocities $v$ and $w$ at the wall are equal to the body-surface velocities due to solid-body rotation. The value of $k$ is set to zero at the wall. Although the specific dissipation rate $\omega$ is theoretically infinite at the wall, the boundary value of $\omega$ is only specified as

$$\omega_{\text{wall}} = (19/9)\left(80\mu_w \big/ \rho d_1^2\right) \qquad (23)$$

where $d_1$ is the distance of the first cell center from the wall.[15] The boundary conditions are also applied for each coarse level of the multigrid.

## Results and Discussion

To verify the present method using the steady coning motions, computations are performed for the ANSR geometries, as shown in Fig. 2. The ANSR projectile consists of a 2-caliber ogive nose with total body lengths of 5 and 9 calibers. Three-dimensional turbulent computations are made with three different c.g. locations shown in Table 1. Then the results are compared with the previous computational results[6] and range data[22] at the Mach numbers 1.8 and 2.5. Five sets of multiblock-structured grids for the full-body configuration are generated to perform a grid refinement study, as shown in Table 2. The body grid (1) of the finest grid, shown in Fig. 3, has 161 node points in the flow direction and 257 and 97 points in the circumferential and radial directions, respectively. The base grid (2) from the center of body base to far field consists of 97 points in the flow direction and 257 and 129 points in the circumferential and radial directions, respectively. Other grids are made by halving the finest grid successively to examine the grid-direction effect. The grids are clustered normal to the surfaces in each direction to ensure the surface grid requirement of the $k$–$\omega$ turbulence model, which is $y^+ \leq 1$ in the first cell for coarse grids 4 and 5 (Ref. 13).

Figure 4 shows the variation of the pitch–damping force and moment coefficients with grid resolution at a forward c.g. location of the 5-caliber body at Mach 2.5. A grid refinement study shows that the difference between grid 1 and grid 2 is less than 1.0% for the pitch–damping force coefficients and 1.5% for the moment coefficients. The variation of force and moment coefficients is more sensitive to the number of grid points in the normal direction rather than in

**Table 1 ANSR projectiles c.g. locations**

| $L/D$ | Forward | Middle | Rearward |
|---|---|---|---|
| 5 | 2.5 | 3.0 | 3.5 |
| 9 | 4.0 | 5.038 | 5.885 |

**Table 2 Grid systems used for ANSR goemetries**

| Grid no. | Size of body grid | Size of base grid | Coarsening direction |
|---|---|---|---|
| 1 | $161 \times 257 \times 97$ | $97 \times 257 \times 129$ | |
| 2 | $161 \times 65 \times 97$ | $97 \times 65 \times 129$ | JM/4 |
| 3 | $161 \times 33 \times 97$ | $97 \times 33 \times 129$ | JM/8 |
| 4 | $161 \times 33 \times 49$ | $97 \times 33 \times 65$ | JM/8, KM/2 |
| 5 | $81 \times 33 \times 49$ | $49 \times 33 \times 65$ | IM/2, JM/8, KM/2 |

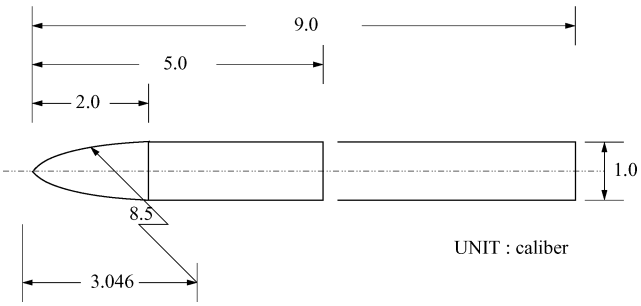


**Fig. 2 ANSR goemetry.**

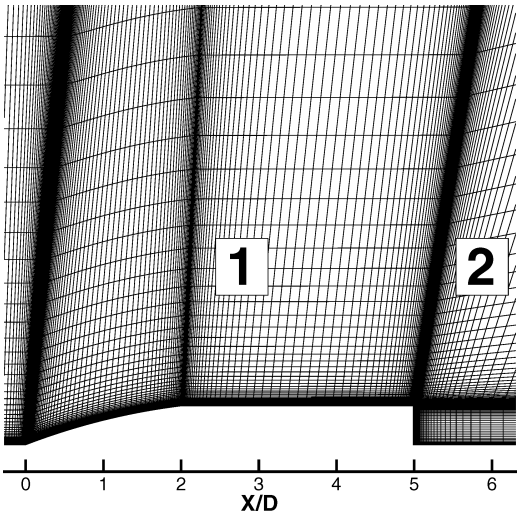


**Fig. 3 Computational grid (grid 1).**

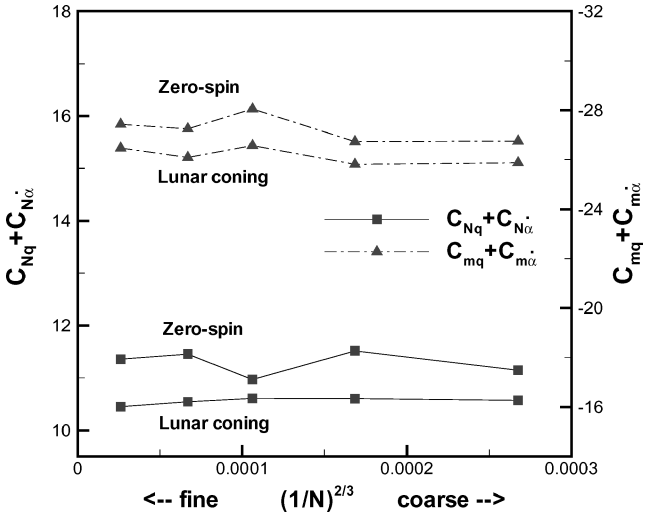


**Fig. 4 Grid convergence of pitch–damping coefficients: $M_\infty = 2.5$ and $L/D = 5$.**

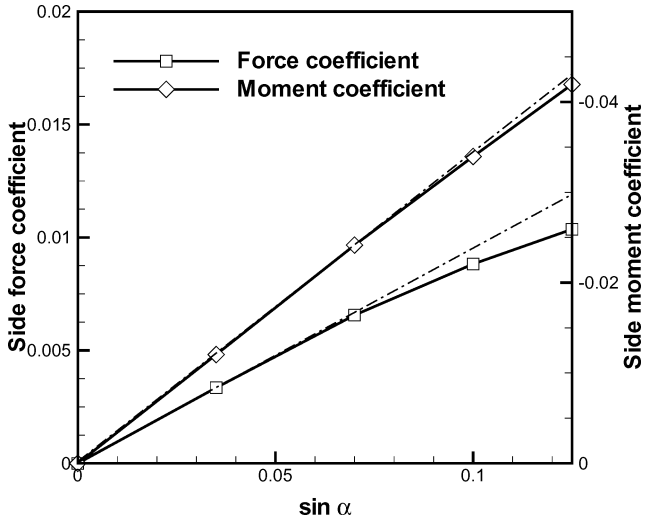


**Fig. 5 Variation of side-force and side-moment coefficients with sine of angle of attack: $M_\infty = 2.5$ and $L/D = 5$.**

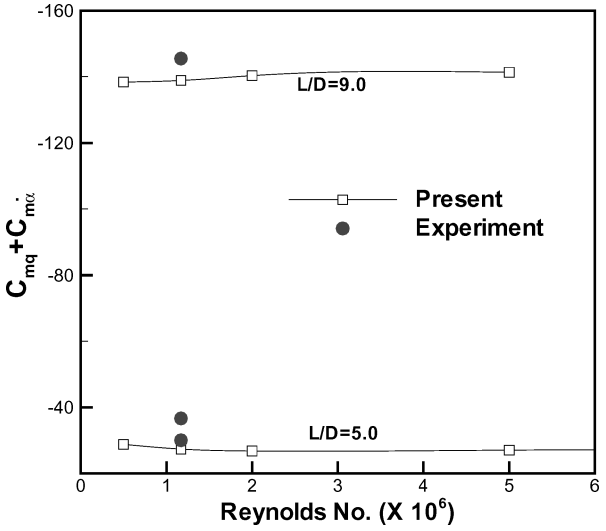


**Fig. 6 Variation of pitch-damping moment coefficient with Reynolds number: $M_\infty = 2.5$ and $L/D = 9$.**

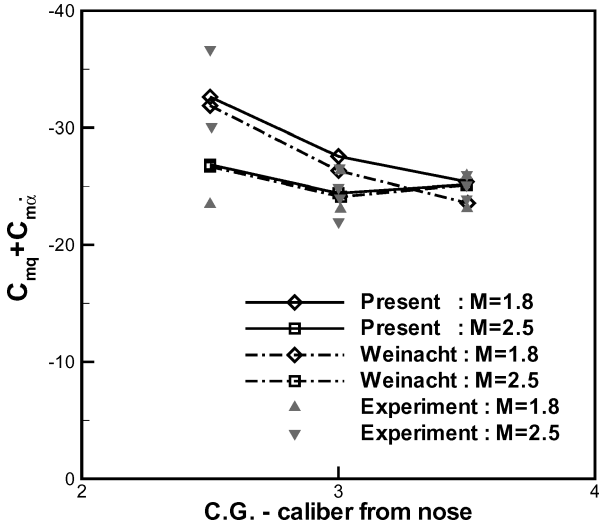


**Fig. 7 Variation of pitch–damping moment coefficient with c.g. location: $L/D = 5$.**

other directions. Although there are several issues for grid independence, such as cell aspect ratio and orthogonality, the number of grid points in the circumferential direction seems to be acceptable for the pitch–damping coefficients. If a grid-independent value is pursued, especially for the Magnus moment coefficient, a grid finer than grid 1 has to be used to capture the boundary-layer distortion due to a roll motion accurately.[9] Unless otherwise stated, results are obtained with grid 2 for all cases. Each of the steady-state calculations required approximately 60–80 min of CPU time on a 24-Pentium 2.4-GHz Linux-cluster to converge the solution to 0.1% variation of the side-moment coefficients.

Note that the side moment relations require the linearity of the force and moment coefficients with $\Omega D/(2U_\infty)$ and $\sin\alpha$. Figure 5 shows the variation of the side force and moments with sine of the angle of attack for a coning rate $\Omega D/(2U_\infty)$ of 0.005. The variation shows the side-force and side-moment coefficients are linearly proportional to the sine of the angle of attack at small angles of attack. As the angle of attack increases, the variation departs from the linear variation. The linearity with a coning rate is valid below 0.01 (Ref. 7). Computations are performed with a coning rate of $\Omega D/(2U_\infty) = 0.005$ and $\alpha = 2$ deg, which are enough to confirm the linearity.

The Reynolds number effect of the turbulent flow computations is examined for both 5- and 9-caliber bodies at Mach 2.5. The range tests were performed for standard sea level conditions and the Reynolds number is $1.17 \times 10^6$ based on the base diameter. Applied are Reynolds numbers based on the base diameter of 0.5, 1.17, 2.0, and $5.0 \times 10^6$. The results in Fig. 6 show that the Reynolds number effect can be negligible at $1.17 \times 10^6$ and higher for the present cases. The pitch damping has been considered as an inviscid phenomenon[6] because the pitch damping results mainly from pressure distribution on the windside and leeside surfaces due to the pitching motion of projectiles. Also note that the viscous effects are significant provided that the magnitude of the pitch damping is small, especially for high supersonic flows.[4] In this study, all other computations are made with a Reynolds number of $1.17 \times 10^6$. Although the freestream conditions can also affect the flowfield solutions for the present $k$–$\omega$ turbulence model, the effect is not considered in this study.

Figures 7 and 8 show the variation of the pitch–damping moment coefficient with c.g. location at Mach numbers 1.8 and 2.5 for the 5 and 9 $L/D$ bodies. The results from the zero-spin coning motion are in good agreement with the parabolized Navier–Stokes (PNS) results (see Ref. 6) and experimental data.[22] It appears that ballistic range data can have scatter of up to 25% or more.[23] Furthermore, the range data at the middle c.g. location in both Figs. 7 and 8 deviate from the trend that appears in the computations and the experiments. The cause of this deviation is unknown, however. The

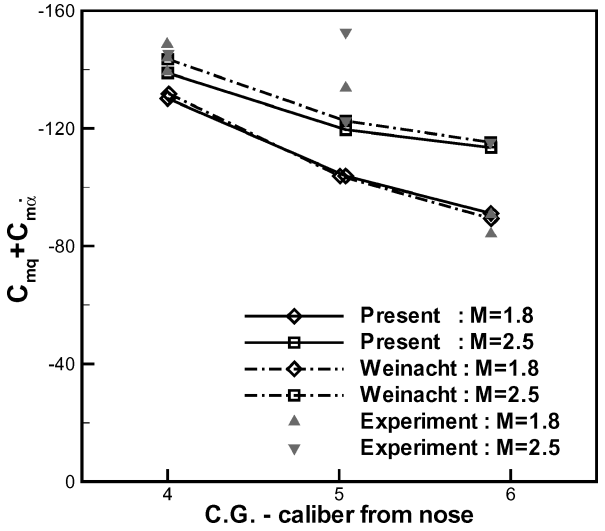


**Fig. 8 Variation of pitch–damping moment coefficient with c.g. location: *L/D* = 9.**

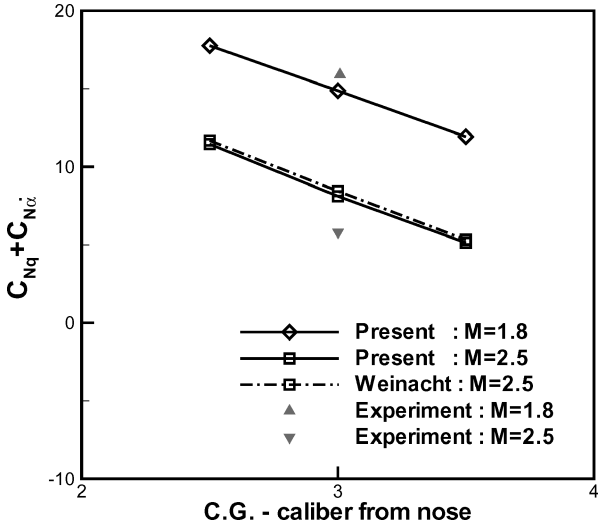


**Fig. 9 Variation of pitch–damping force coefficient with c.g. location: *L/D* = 5.**

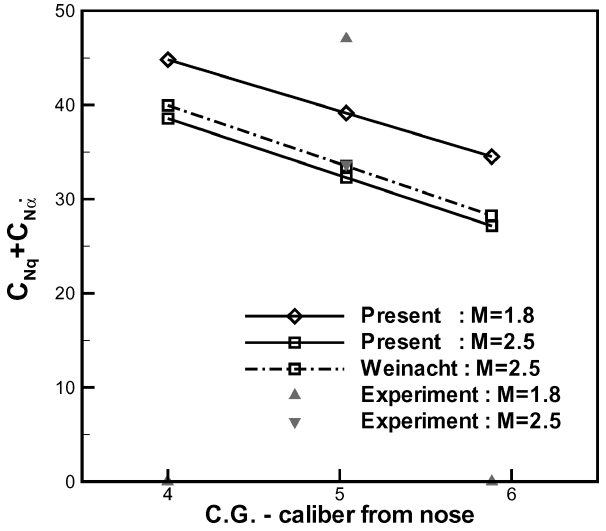


**Fig. 10 Variation of pitch–damping force coefficient with c.g. location: *L/D* = 9.**

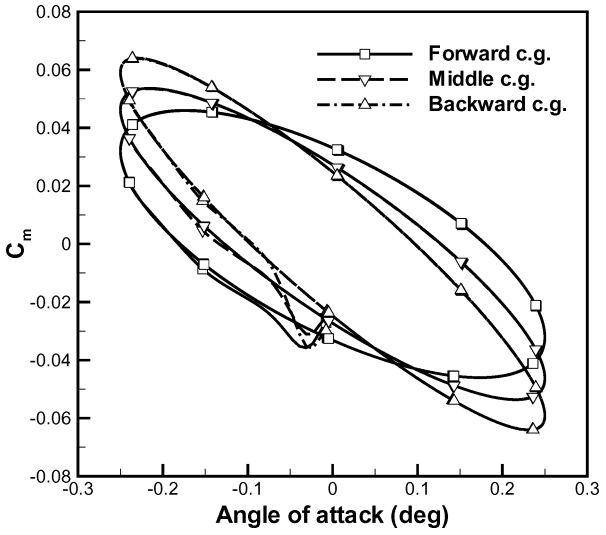


**Fig. 11 Hysteresis loop of pitch–damping moment with c.g. location: $M_\infty$ = 2.5 and *L/D* = 9.**

maximum differences between the full-NS and PNS results are 6.4% at $M = 1.8$ for $L/D = 5$ and 3.3% at $M = 2.5$ for $L/D = 9$. The PNS computations were performed using a shock-fitting procedure and the Baldwin–Lomax algebraic turbulence model. The difference between the present and PNS results is believed to result from the applied grid and numerical algorithms.

Figures 9 and 10 show the variation of the pitch-damping force coefficient with c.g. location at Mach numbers 1.8 and 2.5 for the 5 and 9 $L/D$ bodies. Unlike the static force coefficient, the pitch–damping force coefficient varies linearly with the c.g. location. The linear variation with the c.g. location is verified by the following c.g. translation relations[6,24]:

$$\hat{C}_{N_q} + \hat{C}_{N_{\dot{\alpha}}} = C_{N_q} + C_{N_{\dot{\alpha}}} + s_{\mathrm{cg}} C_{N_\alpha} \tag{24}$$

where $s_{\mathrm{cg}}$ is the c.g. shift in calibers and is positive for a c.g. shift toward the nose. As a result, the slope of the variation with the c.g. location is the normal force coefficient slope $C_{N_\alpha}$, which is independent of the c.g. location. When this relation is used, the slopes calculated are 3.36 for $L/D = 5$ and 6.05 for $L/D = 9$ with 0.5 and 2.5% difference from the PNS predictions, respectively. The variation of the pitch–damping force coefficient shows that the coefficients are in good agreement with the PNS results. Although a small difference in the magnitude can be found, the slope and aspect of the variation of the pitch-damping coefficients obtained from the present steady method in the Cartesian coordinate frame are nearly the same as the referenced PNS results.

As mentioned, the pitch–damping coefficients can be determined by both steady and unsteady prediction methods. The steady prediction of the zero-spin coning motion is theoretically equivalent to the unsteady prediction using the forced harmonic pitching motion.[1] In this work, the unsteady predictions are performed at Mach 2.5 for each c.g. location of the $L/D = 9$ geometry using the unsteady turbulent NS equations. Figure 11 presents the hysteresis loops for the pitch–damping moments of the unsteady simulations for the turbulent flows at zero mean angle of attack. The amplitude of oscillations $\alpha_0$ is set to 0.25 deg, and the computations are performed using 200 time steps per cycle of motion. Displayed are three cycle loops for each time step. The computed moments on the second cycle are not different from the moments on the third cycle for these cases. If the tolerance of convergence, $10^{-2}$, of the normalized L2 norm of density for the unsteady computations is not sufficient, the converged loops cannot be obtained within two or three cycles. Note that the effects of the physical time step and tolerance of convergence were examined to obtain the converged unsteady results (not shown). The pitch–damping moment coefficients are determined by Eq. (4) using the computed moments on the third cycles of the hysteresis loops. When the multigrid algorithm is used, it is found that the numbers of

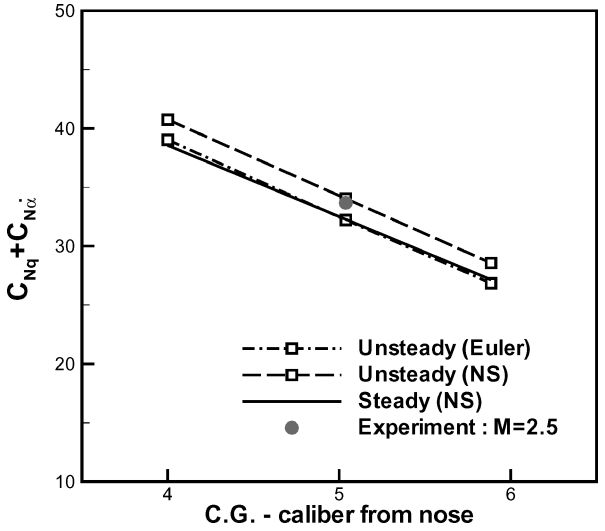


**Fig. 12 Comparison of pitch–damping force coefficients: $M_\infty = 2.5$ and $L/D = 9$.**

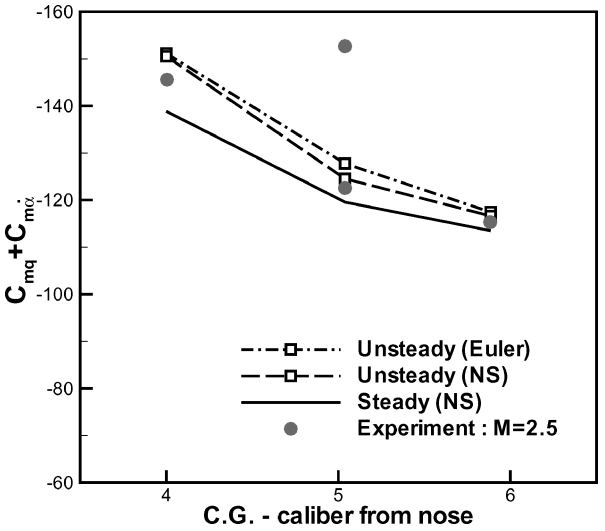


**Fig. 13 Comparison of pitch–damping moment coefficients: $M_\infty = 2.5$ and $L/D = 9$.**

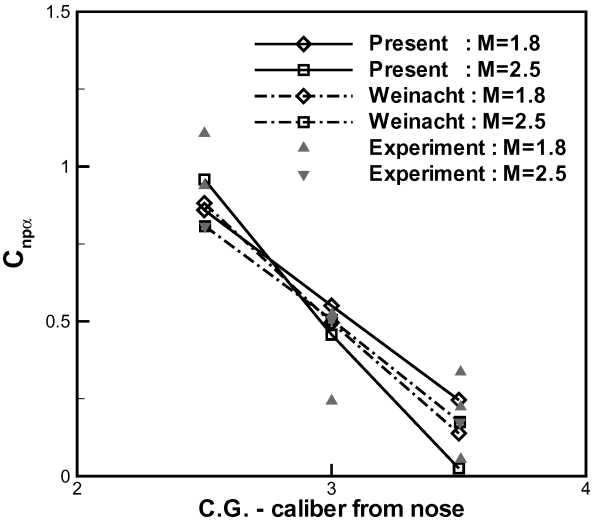


**Fig. 14 Variation of the Magnus moment coefficient: $L/D = 5$.**

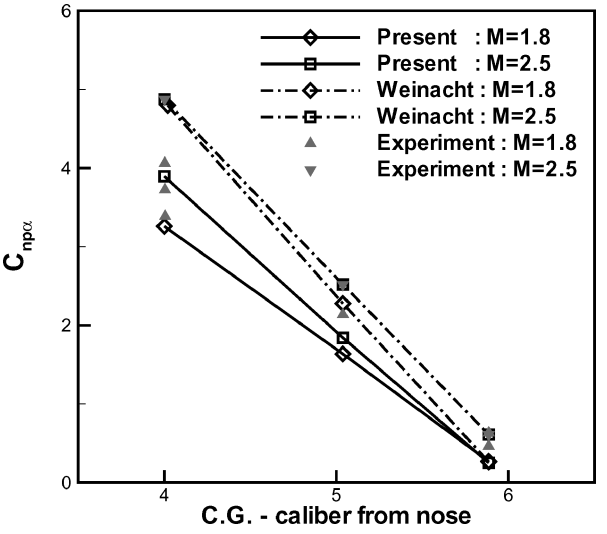


**Fig. 15 Variation of the Magnus moment coefficient: $L/D = 9$.**

multigrid cycles for a physical time step is around 10 for the inviscid cases and 15 for the turbulent computations. Therefore, a single unsteady computation takes about five times as much computing time as a single steady computation for the present computations.

The unsteady Euler and NS predictions in Figs. 12 and 13 are compared with the approximate steady-state NS predictions of the pitch–damping force and moment coefficients. In Fig. 12, the pitch–damping force coefficients obtained from the unsteady Euler simulations are similar to the steady NS results for this case. The unsteady predictions in Fig. 13 yield larger damping for all computed cases, but the variation has the same aspect to the steady turbulent predictions undergoing the zero-spin coning motion. The largest difference between the steady and the unsteady NS results are 4.2% in magnitude for the pitch–damping force coefficients and 8.0% for the pitch–damping moment coefficients. This difference seems to be caused by the linear assumption of the steady prediction method and several nonlinear flow effects. More rigorous study to assess this difference is definitely needed.

Figures 14 and 15 show the variation of the pitch–damping force coefficient with c.g. location at Mach numbers 1.8 and 2.5 for the 5 and 9 $L/D$ bodies. The Magnus force and moment can be obtained from the general unsteady approach[9] using a spinning motion at the angle of attack, although this is not attempted in this study. As a practical method, the Magnus moment is determined by the difference between the lunar coning motion and the zero-spin coning motion. The combination of the coning motion and the spinning motion at an angle of attack produces a Magnus-like moment as well as the Magnus moment itself (see Ref. 6). A grid fine enough to minimize the Magnus-like effect should be used for the steady coning motions. The computational results are within the scatter of the experimental data, although the Magnus moment coefficients are predicted with differences by as much as 30–50% for several computed points compared with the experimental data. This indicates an error in the computed moment when the pitch–damping moment coefficient is predicted by the lunar coning motion. As shown, the magnitudes of the Magnus moments are smaller than 5% of the pitch–damping moment coefficients for the supersonic axisymmetric ANSR geometry. The lunar coning motion, however, is a good alternative for finned projectiles[5] at a supersonic regime because the Magnus moment is relatively small.

## Conclusions

A prediction method for the pitch–damping force and moment coefficients was presented in the unified framework of the turbulent NS equations. Using the relative velocity of the coning motions in the unsteady governing equations enables us to predict the pitch–damping coefficients in a simple manner. The present method was applied to compute the pitch–damping coefficients using the lunar

coning and the zero-spin coning motions. The results were compared with published PNS data and experimental data. The predictions using the unsteady Euler and NS equations were also compared with the steady coning predictions. Although small discrepancies appeared, the overall trend and magnitudes of the steady coning results were in good agreement with the PNS data and the unsteady prediction data. The results showed that the steady approach using the governing equations in the Cartesian coordinate frame can be successfully applied to predict the pitch–damping coefficients. The present approach can also be applied to determine the individual coefficients using the helical motions without difficulty.

## References

[1]Park, S. H., Kim, Y., and Kwon, J. H., "Prediction of Damping Coefficients Using the Unsteady Euler Equations," *Journal of Spacecraft and Rockets*, Vol. 40, No. 3, 2003, pp. 356–362.

[2]Tobak, M., Schiff, L. B., and Peterson, V. L., "Aerodynamics of Bodies of Revolution in Coning Motion," *AIAA Journal*, Vol. 7, No. 1, 1969, pp. 95–99.

[3]Schiff, L. B., "Nonlinear Aerodynamics of Bodies in Coning Motion," *AIAA Journal*, Vol. 10, No. 11, 1972, pp. 1517–1522.

[4]Lin, T. C., "Numerical Study of Re-Entry Vehicle Aerodynamics in Steady Coning Motion," *Journal of Spacecraft and Rockets*, Vol. 18, No. 3, 1981, pp. 228–234.

[5]Weinacht, P., and Sturek, W. B., "Navier–Stokes Predictions of Pitch Damping for Finned Projectiles Using Steady Coning Motion," *Proceedings of the AIAA 8th Applied Aerodynamics Conference*, AIAA, Washington, DC, 1990, pp. 632–642.

[6]Weinacht, P., Sturek, W. B., and Schiff, L. B., "Navier–Stokes Predictions of Pitch Damping for Axisymmetric Projectiles," *Journal of Spacecraft and Rockets*, Vol. 34, No. 6, 1997, pp. 753–761.

[7]Weinacht, P., Sturek, W. B., and Schiff, L. B., "Navier–Stokes Predictions of the Individual Components of the Pitch–Damping Sum," *Journal of Spacecraft and Rockets*, Vol. 35, No. 5, 1998, pp. 598–605.

[8]Qin, N., Ludlow, D. K., Shaw, S. T., Edwards, J. A., and Dupuis, A., "Calculation of Pitch Damping for a Flared Projectile," *Journal of Spacecraft and Rockets*, Vol. 34, No. 4, 1997, pp. 566–568.

[9]Pechier, M., Guillen, P., and Cayzac, R., "Magnus Effect over Finned Projectiles," *Journal of Spacecraft and Rockets*, Vol. 38, No. 4, 2001, pp. 542–549.

[10]Chima, R. V., and Yokota, J. W., "Numerical Analysis of Three-Dimensional Viscous Internal Flows," *AIAA Journal*, Vol. 28, No. 5, 1990, pp. 798–806.

[11]Srinivasan, G. R., Baeder, J. D., Obayashi, S., and McCroskey, W. J., "Flowfield of a Lifting Rotor in Hover: A Navier–Stokes Simulation," *AIAA Journal*, Vol. 30, No. 10, 1992, pp. 2371–2378.

[12]Chen, J. P., Ghosh, A. R., Sreenivas, K., and Whitfield, D. L., "Comparison of Computations Using Navier–Stokes Equations in Rotating and Fixed Coordinates for Flow Through Turbomachinery," AIAA Paper 97-0878, Jan. 1997.

[13]Park, S. H., and Kwon, J. H., "Comparative Study of $k$–$\omega$ Turbulence Models for Transonic Separated Flows," *Proceedings of the Fifth Asian Computational Fluid Dynamics Conference*, ACFD5 and KSCFE, Busan, Republic of Korea, 2003.

[14]Wilcox, D. C., "Reassessment of the Scale-Determining Equation for Advanced Turbulence Models," *AIAA Journal*, Vol. 26, No. 11, 1988, pp. 1299–1310.

[15]Liu, F., and Zheng, X., "A Strongly Coupled Time-Marching Method for Solving the Navier–Stokes and $k$–$\omega$ Turbulence Model Equations with Multigrid," *Journal of Computational Physics*, Vol. 128, No. 2, 1996, pp. 289–300.

[16]Park, S. H., and Kwon, J. H., "On the Dissipation Mechanism of Godunov-Type Schemes," *Journal of Computational Physics*, Vol. 188, No. 2, 2003, pp. 524–542.

[17]Anderson, W. K., Thomas, J. L., and Van Leer, B., "Comparison of Finite Volume Flux Vector Splittings for the Euler Equations," *AIAA Journal*, Vol. 24, No. 9, 1986, pp. 1453–1460.

[18]Sung, C. H., Park, S. H., and Kwon, J. H., "Multigrid Diagonalized ADI Method for Compressible Flows," AIAA Paper 2001-2556, June 2001.

[19]Jameson, A., "Time Dependent Calculations Using Multigrid with Applications to Unsteady Flows Past Airfoils and Wings," AIAA Paper 91-1596, June 1991.

[20]Dubuc, L., Cantariti, F., Woodgate, M., Gribben, B., Badcock, K. J., and Richards, B. E., "Solution of the Unsteady Euler Equations Using an Implicit Dual-Time Method," *AIAA Journal*, Vol. 36, No. 8, 1998, pp. 1417–1424.

[21]Menter, F. R., "Influence of Freestream Values on $k$–$\omega$ Turbulence Model Predictions," *AIAA Journal*, Vol. 30, No. 6, 1992, pp. 1657–1659.

[22]Murphy, C. H., and Schmidt, L. E., "The Effect of Length on the Aerodynamics Characteristics of Bodies of Revolution in Supersonic Flight," U.S. Army Ballistic Research Lab., Rept. 876, Aberdeen Proving Ground, MD, Aug. 1953.

[23]Moore, F. G., and Hymer, T. C., "Semiempirical Prediction of Pitch Damping Moments for Configurations with Flares," *Journal of Spacecraft and Rockets*, Vol. 38, No. 2, 2001, pp. 150–158.

[24]Murphy, C. H., "Free Flight Motion of Symmetric Missiles," U.S. Army Ballistic Research Lab., Rept. 1216, Aberdeen Proving Ground, MD, July 1963.

R. Cummings
*Associate Editor*